Width Difference in the $B-\bar{B}$ System at Next-to-Next-to-Leading Order of QCD

Marvin Gerlach,* Ulrich Nierste,† Vladyslav Shtabovenko,‡ and Matthias Steinhauser§
Institut für Theoretische Teilchenphysik, Karlsruhe Institute of Technology (KIT), 76128 Karlsruhe, Germany

(Received 25 May 2022; revised 6 July 2022; accepted 5 August 2022; published 31 August 2022)

We extend the theoretical prediction for the width difference $\Delta\Gamma_q$ in the mixing of neutral B mesons in the Standard Model to next-to-next-to-leading order in α_s. To this aim, we calculate three-loop diagrams with two $|\Delta B| = 1$ current-current operators analytically. In the matching between $|\Delta B| = 1$ and $|\Delta B| = 2$ effective theories, we regularize the infrared divergences dimensionally and take into account all relevant evanescent operators. Further elements of the calculation are the two-loop renormalization matrix Z_{ij} for the $|\Delta B| = 2$ operators and the $\mathcal{O}(\alpha_s^2)$ corrections to the finite renormalization that ensures the $1/m_b$ suppression of the operator R_0 at two-loop order. Our theoretical prediction reads $\Delta\Gamma_s/\Delta M_s = (4.33 \pm 0.93) \times 10^{-3}$ if expressed in terms of the bottom mass in the $\overline{\text{MS}}$ scheme and $\Delta\Gamma_s/\Delta M_s = (4.20 \pm 0.95) \times 10^{-3}$ for the use of the potential-subtracted mass. While the controversy on $|V_{cb}|$ affects both $\Delta\Gamma_s$ and ΔM_s, the ratio $\Delta\Gamma_s/\Delta M_s$ is not affected by the uncertainty in $|V_{cb}|$.

DOI: 10.1103/PhysRevLett.129.102001

Introduction.—The weak interaction of the Standard Model (SM) permits transitions between a neutral B_q meson and its antiparticle $\bar{B}_q$, where $q = d$ or s. The corresponding transition amplitude is mediated by box diagrams with W bosons and up-type quarks u, c, or t on the internal lines. The time evolution of the two-state system $(|B_q\rangle, |\bar{B}_q\rangle)$ is governed by two Hermitian 2×2 matrices, the mass matrix M^q, and the decay matrix Γ^q. By diagonalizing $M^q - i\Gamma^q/2$, one finds the mass eigenstates $|B_L^q\rangle$ and $|B_H^q\rangle$ expressed in terms of the flavor eigenstates $|B_q\rangle$, $|\bar{B}_q\rangle$. There are three observables: the mass and width differences ΔM_q and $\Delta\Gamma_q$ among the mass eigenstates, as well as the CP asymmetry in flavor-specific decays, a_{fs}^q. Experimentally, ΔM_q is read off from the $B_q - \bar{B}_q$ oscillation frequency, $\Delta\Gamma_q$ is found by measuring lifetimes in different decay modes, and a_{fs}^q is usually measured through the time-dependent CP asymmetry in semileptonic B_q decays. These observables are related to the off-diagonal elements of M^q and Γ^q as follows:

$$\Delta M_q \simeq 2|M_{12}^q|, \qquad \frac{\Delta\Gamma_q}{\Delta M_q} = -\text{Re}\frac{\Gamma_{12}^q}{M_{12}^q}, \qquad a_{\text{fs}}^q = \text{Im}\frac{\Gamma_{12}^q}{M_{12}^q}, \tag{1}$$

with $|\Delta\Gamma_q| \simeq 2|\Gamma_{12}^q|$. M_{12}^q is sensitive to new physics mediated by heavy particles, while Γ_{12}^q probes the effects of light new particles with feeble couplings (see, e.g., Refs. [1,2]). However, a better knowledge of Γ_{12}^q will also help to reveal new physics in M_{12}^q: Inclusive and exclusive semileptonic B decays give different values for the element $|V_{cb}|$ of the Cabibbo-Kobayashi-Maskawa (CKM) matrix, leading to an $\mathcal{O}(15\%)$ uncertainty onto the CKM factor $(V_{tb}V_{tq}^*)^2$ of M_{12}^q, which cancels from the ratio $\Delta\Gamma_q/\Delta M_q$ in Eq. (1).

The measurements of LHCb [3], CMS [4], ATLAS [5], CDF [6], and DØ [7] combine to

$$\Delta\Gamma_s^{\text{exp}} = (0.082 \pm 0.005)\ \text{ps}^{-1}\ [8], \tag{2}$$

while $\Delta\Gamma_d^{\text{exp}}$ is consistent with zero. The precise value in Eq. (2) calls for a better SM prediction. We specify to $q = s$ from now on.

The SM predictions for Γ_{12}^s are calculated from the dispersive part of the $B_s \leftrightarrow \bar{B}_s$ amplitude. To properly accommodate strong interaction effects from different energy scales, one employs two operator product expansions (OPEs). First, one matches the SM to an effective theory with $|\Delta B| = 1$ operators [9], where B is the beauty quantum number. The operators with the largest coefficients are the current-current operators $Q_{1,2}$ describing tree-level b decays. The effective $|\Delta B| = 1$ Hamiltonian is known to the next-to-leading (NLO) [10–12] and next-to-next-to-leading order (NNLO) [13–15] of quantum chromodynamics (QCD). Second, one employs the heavy quark expansion (HQE) [16–24] (cf. also Ref. [25] for a review), which expresses the $B_s \leftrightarrow \bar{B}_s$ transition amplitude as a series in Λ_{QCD}/m_b, where $\Lambda_{\text{QCD}} \sim 400$ MeV is the fundamental scale of QCD and m_b is the b quark mass. The HQE involves local $|\Delta B| = 2$ operators; the corresponding

Wilson coefficients are found from the $\Delta B = 2$ amplitude calculated in both the $|\Delta B| = 1$ and $|\Delta B| = 2$ theories to the desired order in α_s.

The state of the art is as follows: QCD corrections to Γ_{12}^s are only known for the leading term of the $\Lambda_{\rm QCD}/m_b$ expansion ("leading power"). These include NLO QCD corrections to the contributions with current-current and chromomagnetic penguin operators [26–29], the corresponding NNLO corrections (and NLO corrections involving four-quark penguin operators) proportional to the number N_f of active quark flavors [30–32], as well as NLO results with one current-current and one penguin operator [33] or two penguin operators [34]. The latter paper also presents two-loop results with one or two chromomagnetic penguin operators being part of the NNLO and N^{3}LO contributions. (The four-quark penguin operators $Q_{3\text{–}6}$ have Wilson coefficients which are much smaller than those of $Q_{1,2}$, and the chromomagnetic penguin operator contributes with a suppression factor of α_s.) The corrections of Ref. [30] and Refs. [33,34] have been calculated as an expansion in m_c/m_b to first and second order, respectively. $\Delta\Gamma_s/\Delta M_s$ further involves a well-computed ratio of two hadronic matrix elements [35–37]. The contribution to Γ_{12}^s being subleading in $\Lambda_{\rm QCD}/m_b$ is only known to the LO of QCD [38], and the hadronic matrix elements still have large errors [39].

Both the described perturbative contribution and the power-suppressed term have theoretical uncertainties exceeding the experimental error in Eq. (2). In this Letter, we present NNLO QCD corrections to the numerically dominant contribution with two current-current operators and reduce the perturbative uncertainty of the leading-power term to the level of the experimental error.

Calculation.—To obtain $\Delta\Gamma_s/\Delta M_s$, we use the known two-loop QCD corrections to M_{12}^s from Ref. [11]. It is convenient to decompose Γ_{12}^s according to the CKM structures

$$\Gamma_{12}^s = -(\lambda_c^s)^2\Gamma_{12}^{cc} - 2\lambda_c^s\lambda_u^s\Gamma_{12}^{uc} - (\lambda_u^s)^2\Gamma_{12}^{uu}, \tag{3}$$

where $\lambda_a^s = V_{as}^* V_{ab}$ with $a = u,\ c$. In a first step, we integrate out all degrees of freedom heavier than the bottom quark mass m_b, so that the dynamical degrees of freedom are given by the five lightest quarks and the gluons. We adopt the operator basis of the $|\Delta B| = 1$ theory from Ref. [40], matched to the Standard Model at the scale $\mu_0 \approx 2m_W \approx m_t(m_t)$. Renormalization group running determines the couplings of the effective operators at the scale μ_1 of the order m_b.

Next, we perform a HQE, which allows us to write Γ_{12}^s as an expansion in $1/m_b$. At each order, Γ_{12}^s is expressed as a sum of Wilson coefficients multiplying respective operator matrix elements, computed using lattice gauge theory [35] or QCD sum rules [36,37]. To leading order in the $1/m_b$ expansion, we have

$$\Gamma_{12}^{ab} = \frac{G_F^2 m_b^2}{24\pi M_{B_s}}\left[H^{ab}(z)\langle B_s|Q|\bar{B}_s\rangle + \tilde{H}_S^{ab}(z)\langle B_s|\tilde{Q}_S|\bar{B}_s\rangle\right] + \mathcal{O}(\Lambda_{\rm QCD}/m_b), \tag{4}$$

where $ab \in \{cc, uc, uu\}$. G_F is the Fermi constant and M_{B_s} is the mass of the B_s meson. The topic of this Letter is the computation of the matching coefficients H^{ab} and $\tilde{H}_S^{ab}$ to next-to-next-to-leading order (NNLO) in the strong coupling constant α_s. They depend on $z = m_c^2/m_b^2$. For the $\Delta B = 1$ theory, one distinguishes current-current and penguin operators. At leading and next-to-leading orders, the current-current operators provide about 90% of the total contribution to Γ_{12}^{ab} [34]. Thus, we restrict ourselves to the current-current contributions.

Our NNLO calculation involves several challenges. First, it is necessary to perform a three-loop calculation of the amplitude $b\bar{s} \to \bar{b}s$ in the $\Delta B = 1$ theory. Sample Feynman diagrams are shown in Fig. 1. In total, about 20 000 three-loop diagrams have to be considered, which requires an automated setup for the computation [41–44]. For the leading term in the HQE, we are allowed to set the momentum of the strange quark to zero. Furthermore, we expand in the charm quark mass up to second order, [45] which reduces the integrals to on-shell two-point functions. The propagators inside the loop diagrams are either massless or carry the mass m_b. All occurring integrals are reduced [46–48] to 23 genuine three-loop master integrals and calculated analytically [49–55].

On the $\Delta B = 2$ side, a two-loop calculation is necessary (cf. Fig. 1), where one encounters three physical and 17 evanescent operators (cf. Ref. [34]). One must compute the corresponding renormalization constants for the operator mixing up to two-loop order.

The calculation of the $\Delta B = 2$ matrix elements entails a field theoretical subtlety. In four dimensions there are only two physical operators, whereas for the calculation in d dimensions three have to be considered. For our calculation, it is convenient to choose Q, $\tilde{Q}_S$, and R_0 [34] with

$$R_0 = Q_S + \alpha_1\tilde{Q}_S + \frac{1}{2}\alpha_2 Q. \tag{5}$$

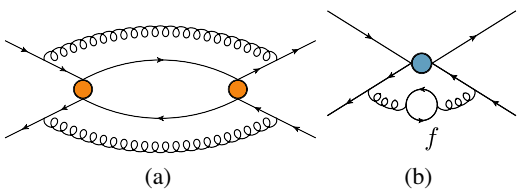

FIG. 1. Sample Feynman diagrams in the $\Delta B = 1$ and $\Delta B = 2$ theories with $f = u,\ d,\ s,\ c,\ b$. Solid and curly lines represent quarks and gluons, respectively. The orange and blue blobs indicate operator insertions.

At lowest order in α_s, we have $\alpha_1 = \alpha_2 = 1$, and the matrix element of R_0 is $1/m_b$ suppressed in four dimensions. At higher orders, the quantities α_1 and α_2 are chosen such that the $1/m_b$ suppression is maintained. The one-loop corrections and the fermionic two-loop terms have been presented in Refs. [26] and [30], respectively. For our NNLO calculation, the α_s^2 corrections to α_1 and α_2 are needed.

The $1/m_b$ suppression of $\langle R_0 \rangle$ beyond tree level is manifest only if one is able to distinguish between ultraviolet (UV) and infrared (IR) divergences, e.g., by regularizing the latter using a gluon mass. Otherwise, R_0 develops an unphysical evanescent piece E_{R_0} that scales as m_b^0 [34] and hence must be included in the definition of R_0 to obtain correct matching coefficients. One cannot isolate E_{R_0} from R_0 at the operator level, but one can distinguish evanescent and physical pieces in the matrix elements: We use R_0 from Eq. (5) *including* the finite UV renormalization encoded in α_1 and α_2 in our matching calculation. To this end, we have first calculated the linear combination of the renormalized two-loop matrix elements $\langle Q \rangle^{(2)}$, $\langle Q_S \rangle^{(2)}$, and $\langle \tilde{Q}_S \rangle^{(2)}$ as given in Eq. (5). Using a gluon mass along the lines of Ref. [56] and Feynman gauge, we observe that each of the individual matrix elements becomes manifestly finite upon UV renormalization. α_1 and α_2 to order α_s^2 are extracted from the requirement that the linear combination must vanish in the limit $m_b \to \infty$.

The matching between the $|\Delta B| = 1$ and $|\Delta B| = 2$ effective theories is conceptually simple in the case where IR divergences are not regularized dimensionally. In this case, the UV renormalization renders amplitudes of both theories manifestly finite, allowing us to take the limit $d \to 4$, where all matrix elements of evanescent operators vanish. However, for technical reasons we prefer to use $\epsilon = \epsilon_{\mathrm{UV}} = \epsilon_{\mathrm{IR}}$, which simplifies the evaluation of the amplitudes but complicates the matching. Following Ref. [57], we need to extend the leading order (LO) matching to $\mathcal{O}(\epsilon^2)$ and the NLO matching to $\mathcal{O}(\epsilon)$ in order to determine the NNLO matching coefficients. Furthermore, we need to determine the matching coefficients of both physical and evanescent operators: Since the UV-renormalized amplitudes still contain IR poles, we must keep all matrix elements of evanescent operators until the very end. A powerful cross-check of this procedure is the explicit cancellation of the remaining IR ϵ poles and of the QCD gauge parameter ξ in the matching.

Results.—For our numerical analysis, we use the input values listed in Table I and the $|\Delta B| = 1$ Wilson coefficients from Refs. [13–15], and we calculate the running and decoupling of quark masses and α_s with `RunDec` [58].

In the following, we present the NNLO predictions in three different renormalization schemes for the overall factor m_b^2 [cf. Eq. (4)], whereas the quantity z and the strong coupling constant are defined in the $\overline{\mathrm{MS}}$ scheme. The overall factor m_b^2 is defined in the $\overline{\mathrm{MS}}$ scheme, as a pole mass, or as a potential-subtracted (PS) mass [62]. The latter is an example of a so-called threshold mass, with similar properties as the pole mass, but is nevertheless of short-distance nature. $H^{ab}(z)$ and $\tilde{H}_S^{ab}(z)$ are adapted accordingly, so that the scheme dependence of Γ_{12}^s is $\mathcal{O}(\alpha_s^3)$. Several renormalization and matching scales enter the prediction for the width difference. We choose $\mu_0 = 165$ GeV for the matching scale between the SM and the $|\Delta B| = 1$ theory. In our numerical analysis, we choose $\mu_1 = \mu_b = \mu_c$ (the renormalization scales at which $\bar{m}_b$ and $\bar{m}_c$ are defined) and vary μ_1 between 2.1 GeV and 8.4 GeV with a central scale $\mu_1 = 4.2$ GeV. In our analysis, we set $\mu_2 = m_b^{\mathrm{pole}} = 4.75$ GeV. It has to be kept fixed, because the μ_2 dependence only cancels in the products of $H^{ab}(z)$ and $\tilde{H}_S^{ab}(z)$ with their respective matrix elements.

TABLE I. Input parameters for the numerical analysis. The matrix elements of Q and $\tilde{Q}_S$ are parametrized in terms of f_{B_s}, B_{B_s}, and $\tilde{B}'_{S,B_s}$. The values of the quark masses imply $\bar{z} = 0.04956$, $m_b^{\mathrm{pole}} = 4.75$ GeV, and $m_b^{\mathrm{PS}} = 4.479$ GeV (for a factorization scale $\mu_f = 2$ GeV) at NNLO. Numerical results for the matrix elements of the $1/m_b$ suppressed corrections can be found in Ref. [39].

$\alpha_s(M_Z) = 0.1179 \pm 0.001$	[59]
$m_c(3\ \mathrm{GeV}) = 0.993 \pm 0.008$ GeV	[60]
$m_b(m_b) = 4.163 \pm 0.016$ GeV	[60]
$m_t^{\mathrm{pole}} = 172.9 \pm 0.4$ GeV	[59]
$M_{B_s} = 5366.88$ MeV	[59]
$B_{B_s} = 0.813 \pm 0.034$	[35]
$\tilde{B}'_{S,B_s} = 1.31 \pm 0.09$	[35]
$f_{B_s} = 0.2307 \pm 0.0013$ GeV	[61]

We now discuss the results for $\Delta\Gamma_s/\Delta M_s$. In our three schemes, we have

$$\begin{aligned}
\frac{\Delta\Gamma_s}{\Delta M_s} &= (3.79^{+0.53}_{-0.58\,\mathrm{scale}}{}^{+0.09}_{-0.19\,\mathrm{scale},1/m_b} \pm 0.11_{B\tilde{B}_S} \\
&\quad \pm 0.78_{1/m_b} \pm 0.05_{\mathrm{input}}) \times 10^{-3}\ (\mathrm{pole}), \\
\frac{\Delta\Gamma_s}{\Delta M_s} &= (4.33^{+0.23}_{-0.44\,\mathrm{scale}}{}^{+0.09}_{-0.19\,\mathrm{scale},1/m_b} \pm 0.12_{B\tilde{B}_S} \\
&\quad \pm 0.78_{1/m_b} \pm 0.05_{\mathrm{input}}) \times 10^{-3}\ (\overline{\mathrm{MS}}), \\
\frac{\Delta\Gamma_s}{\Delta M_s} &= (4.20^{+0.36}_{-0.39\,\mathrm{scale}}{}^{+0.09}_{-0.19\,\mathrm{scale},1/m_b} \pm 0.12_{B\tilde{B}_S} \\
&\quad \pm 0.78_{1/m_b} \pm 0.05_{\mathrm{input}}) \times 10^{-3}\ (\mathrm{PS}),
\end{aligned} \tag{6}$$

where the subscripts indicate the source of the various uncertainties. The dominant uncertainty comes from the matrix elements of the power-suppressed corrections ("$1/m_b$") [35,39] followed by the renormalization scale uncertainty from the variation of μ_1 in the leading-power term ("scale"). The uncertainties from the leading-power bag parameters ("$B\tilde{B}_S$") and from the scale variation in the

$1/m_b$ piece ("scale, $1/m_b$") are much smaller, and the variation of the remaining input parameters ("input") is of minor relevance.

In Fig. 2, we show the dependence of $\Delta\Gamma_s/\Delta M_s$ on the simultaneously varied renormalization scales $\mu_1 = \mu_b = \mu_c$ for the $\overline{\rm MS}$ and PS schemes. The small contributions involving four-quark penguin operators are only included at NLO in both the NLO and NNLO curves. Dotted, dashed, and solid curves correspond to the LO, NLO, and NNLO results, respectively. In both schemes, one observes a clear stabilization of the μ_1 dependence after including higher orders. Furthermore, we observe that the NNLO predictions (solid lines) in both schemes are close together, which demonstrates the expected reduction of the scheme dependence. In the $\overline{\rm MS}$ scheme, we observe that the LO and NLO curves intersect close to the central scale. As a consequence, the NLO corrections are relatively small, and the NNLO contributions are of comparable size. Close to 9 GeV, the NNLO contribution is zero, and the NLO corrections amount to about +21%. At the same time, the NNLO predictions for $\mu_1 = 4.2$ GeV and $\mu_1 = 9$ GeV differ only by +5% and +9% in the $\overline{\rm MS}$ and PS schemes, respectively. Note that in the $\overline{\rm MS}$ scheme, the scale dependence of the leading-power term drops from $^{+0}_{-29}\%$ at NLO to $^{+5}_{-10}\%$ at NNLO and is now of the same order of magnitude as the $\pm 6\%$ experimental error in Eq. (2). In the PS scheme, the scale uncertainty is of the same order of magnitude as in the $\overline{\rm MS}$ scheme. Note that the scheme dependence inferred from the $\overline{\rm MS}$ and PS central values in Eq. (6) is only 3%. Equation (6) clearly shows that one needs better results for the $1/m_b$ matrix elements. A meaningful lattice-continuum matching calls for NLO corrections to the power-suppressed terms, which will further reduce the uncertainty labeled with "scale, $1/m_b$."

For the pole scheme, we only show the NNLO prediction in Fig. 2. While we also see a relatively mild dependence on μ_1, the corresponding solid curve lies significantly below the predictions in the $\overline{\rm MS}$ and PS schemes. This feature can be traced back to the large two-loop corrections in the relation between the $\overline{\rm MS}$ and the pole bottom quark mass affecting NNLO contributions as much as the genuine NNLO corrections, underpinning the well-known issues with quark pole masses [63–65]. For this reason, we recommend not using the pole scheme for the prediction of $\Delta\Gamma_s$.

The most precise prediction for $\Delta\Gamma_s$ is obtained from the results in Eq. (6) combined with the experimental result [66] $\Delta M_s^{\rm exp} = 17.7656 \pm 0.0057\ {\rm ps}^{-1}$. Upon adding the various uncertainties in quadrature, symmetrizing the scale dependence and averaging the results from the $\overline{\rm MS}$ and PS schemes, we obtain

$$\Delta\Gamma_s = (0.076 \pm 0.017)\ {\rm ps}^{-1}. \tag{7}$$

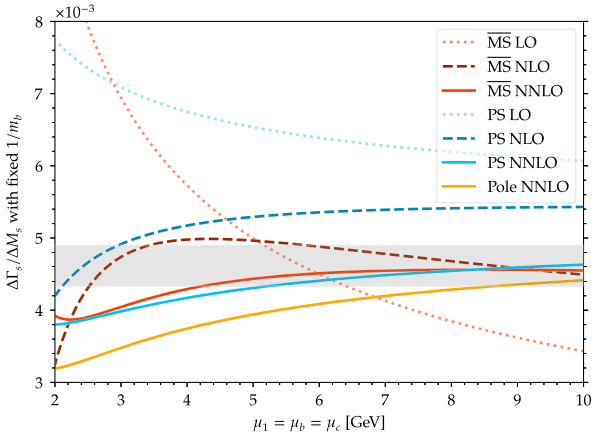

FIG. 2. Renormalization scale dependence at LO, NLO, and NNLO for the $\overline{\rm MS}$ and PS schemes. The scale in the power-suppressed terms is kept fixed. The gray band represents the experimental result.

The comparison to Eq. (2) shows that the uncertainty is only about 3 times bigger than that from experiment and is dominated by the $1/m_b$ corrections.

In Fig. 3, we confront our predictions for the ratio $\Delta\Gamma_s/\Delta M_s$ in the $\overline{\rm MS}$ scheme (green band) with the individual predictions of $\Delta\Gamma_s$ and ΔM_s. The latter are dominated by the uncertainty in the CKM matrix element V_{ts} which is obtained from V_{cb} through CKM unitarity and cancels in the ratio. Figure 3 illustrates this feature with $|V_{cb}^{\rm incl}| = 42.16(51) \times 10^{-3}$ from Ref. [67] and $|V_{cb}^{\rm excl}| = 39.36(68) \times 10^{-3}$ from Ref. [68]. The current experimental results for $\Delta\Gamma_s$ and ΔM_s are indicated by the black bar. Once the prediction of $\Delta\Gamma_s/\Delta M_s$ is improved further, it will be possible to test the SM without CKM uncertainty,

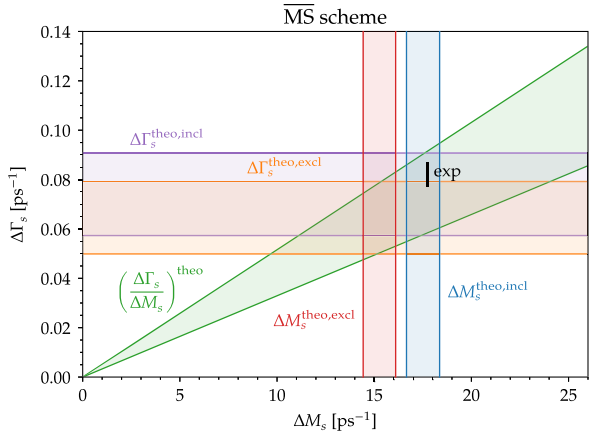

FIG. 3. $\Delta\Gamma_s$ versus ΔM_s. The $|V_{cb}|$ controversy (red vs blue vertical and orange vs purple horizontal strips) prevents any conclusion on possible new physics in ΔM_s. A combined analysis of ΔM_s and $\Delta\Gamma_s$ adds important information, because the SM prediction of $\Delta\Gamma_s/\Delta M_s$ (green wedge) is independent of $|V_{cb}|$.

and with progress on $|V_{cb}|$, one will be able to constrain new physics in ΔM_s and $\Delta\Gamma_s$ individually.

Conclusions.—The SM prediction of $\Delta\Gamma_s/\Delta M_s$ based on the long-standing NLO calculation has two sources of uncertainty which exceed the experimental error: the hadronic matrix elements of the power-suppressed operators and the perturbative coefficients, as inferred from the scale and scheme dependence of the calculated result. With the NNLO calculation presented here, we have brought the latter uncertainty to the level of the accuracy of the experimental result. For this we had to calculate 20 000 three-loop diagrams and to solve subtle problems related to the interplay of infrared divergences and evanescent operators. We have pointed out that $\Delta\Gamma_s$ adds information to the usual study of ΔM_s, because both quantities probe different new-physics scenarios and $|V_{cb}|$ drops out in the ratio $\Delta\Gamma_s/\Delta M_s$.

We thank Artyom Hovhannisyan and Matthew Wingate for useful discussions, and we are grateful to Erik Panzer and Oliver Schnetz for helpful advice regarding the calculation of the master integrals and the simplification of the obtained results with `HyperInt` and `HyperLogProcedures`. V. S. thanks David Broadhurst for enlightening discussions on iterated integrals. This research was supported by the Deutsche Forschungs gemeinschaft (DFG, German Research Foundation) under Grant No. 396021762—TRR 257 "Particle Physics Phenomenology after the Higgs Discovery." The Feynman diagrams were drawn with the help of Axodraw [69] and JaxoDraw [70].

*gerlach.marvin@protonmail.com
†ulrich.nierste@kit.edu
‡v.shtabovenko@kit.edu
§matthias.steinhauser@kit.edu

[1] G. Elor, M. Escudero, and A. E. Nelson, Phys. Rev. D **99**, 035031 (2019).
[2] G. Alonso-Álvarez, G. Elor, and M. Escudero, Phys. Rev. D **104**, 035028 (2021).
[3] R. Aaij *et al.* (LHCb Collaboration), Eur. Phys. J. C **79**, 706 (2019); **80**, 601(E) (2020).
[4] A. M. Sirunyan *et al.* (CMS Collaboration), Phys. Lett. B **816**, 136188 (2021).
[5] G. Aad *et al.* (ATLAS Collaboration), Eur. Phys. J. C **81**, 342 (2021).
[6] T. Aaltonen *et al.* (CDF Collaboration), Phys. Rev. Lett. **109**, 171802 (2012).
[7] V. M. Abazov *et al.* (D0 Collaboration), Phys. Rev. D **85**, 032006 (2012).
[8] H. F. A. G. (HFLAV Collaboration), https://hflav-eos.web.cern.ch/hflav-eos/osc/PDG_2020/#DMS.
[9] F. J. Gilman and M. B. Wise, Phys. Rev. D **20**, 2392 (1979).
[10] A. J. Buras and P. H. Weisz, Nucl. Phys. **B333**, 66 (1990).
[11] A. J. Buras, M. Jamin, and P. H. Weisz, Nucl. Phys. **B347**, 491 (1990).
[12] A. J. Buras, M. Jamin, M. E. Lautenbacher, and P. H. Weisz, Nucl. Phys. **B370**, 69 (1992); **B375**, 501(E) (1992).
[13] M. Gorbahn and U. Haisch, Nucl. Phys. **B713**, 291 (2005).
[14] P. Gambino, M. Gorbahn, and U. Haisch, Nucl. Phys. **B673**, 238 (2003).
[15] M. Gorbahn, U. Haisch, and M. Misiak, Phys. Rev. Lett. **95**, 102004 (2005).
[16] V. A. Khoze and M. A. Shifman, Sov. Phys. Usp. **26**, 387 (1983).
[17] M. A. Shifman and M. B. Voloshin, Sov. J. Nucl. Phys. **41**, 120 (1985).
[18] V. A. Khoze, M. A. Shifman, N. G. Uraltsev, and M. B. Voloshin, Sov. J. Nucl. Phys. **46**, 112 (1987).
[19] J. Chay, H. Georgi, and B. Grinstein, Phys. Lett. B **247**, 399 (1990).
[20] I. I. Y. Bigi and N. G. Uraltsev, Phys. Lett. B **280**, 271 (1992).
[21] I. I. Y. Bigi, N. G. Uraltsev, and A. I. Vainshtein, Phys. Lett. B **293**, 430 (1992); **297**, 477(E) (1992).
[22] I. I. Y. Bigi, M. A. Shifman, N. G. Uraltsev, and A. I. Vainshtein, Phys. Rev. Lett. **71**, 496 (1993).
[23] B. Blok, L. Koyrakh, M. A. Shifman, and A. I. Vainshtein, Phys. Rev. D **49**, 3356 (1994); **50**, 3572(E) (1994).
[24] A. V. Manohar and M. B. Wise, Phys. Rev. D **49**, 1310 (1994).
[25] A. Lenz, Int. J. Mod. Phys. A **30**, 1543005 (2015).
[26] M. Beneke, G. Buchalla, C. Greub, A. Lenz, and U. Nierste, Phys. Lett. B **459**, 631 (1999).
[27] M. Ciuchini, E. Franco, V. Lubicz, F. Mescia, and C. Tarantino, J. High Energy Phys. 08 (2003) 031.
[28] M. Beneke, G. Buchalla, A. Lenz, and U. Nierste, Phys. Lett. B **576**, 173 (2003).
[29] A. Lenz and U. Nierste, J. High Energy Phys. 06 (2007) 072.
[30] H. M. Asatrian, A. Hovhannisyan, U. Nierste, and A. Yeghiazaryan, J. High Energy Phys. 10 (2017) 191.
[31] H. M. Asatrian, H. H. Asatryan, A. Hovhannisyan, U. Nierste, S. Tumasyan, and A. Yeghiazaryan, Phys. Rev. D **102**, 033007 (2020).
[32] A. Hovhannisyan and U. Nierste, J. High Energy Phys. 06 (2022) 090.
[33] M. Gerlach, U. Nierste, V. Shtabovenko, and M. Steinhauser, J. High Energy Phys. 07 (2021) 043.
[34] M. Gerlach, U. Nierste, V. Shtabovenko, and M. Steinhauser, J. High Energy Phys. 04 (2022) 006.
[35] R. J. Dowdall, C. T. H. Davies, R. R. Horgan, G. P. Lepage, C. J. Monahan, J. Shigemitsu, and M. Wingate, Phys. Rev. D **100**, 094508 (2019).
[36] M. Kirk, A. Lenz, and T. Rauh, J. High Energy Phys. 12 (2017) 068; 06 (2020) 162(E).
[37] D. King, A. Lenz, and T. Rauh, J. High Energy Phys. 06 (2022) 134.
[38] M. Beneke, G. Buchalla, and I. Dunietz, Phys. Rev. D **54**, 4419 (1996); **83**, 119902(E) (2011).
[39] C. T. H. Davies, J. Harrison, G. P. Lepage, C. J. Monahan, J. Shigemitsu, and M. Wingate (HPQCD Collaboration), Phys. Rev. Lett. **124**, 082001 (2020).
[40] K. G. Chetyrkin, M. Misiak, and M. Munz, Nucl. Phys. **B520**, 279 (1998).

[41] P. Nogueira, J. Comput. Phys. **105**, 279 (1993).
[42] M. Gerlach, F. Herren, and M. Lang, arXiv:2201.05618.
[43] R. Harlander, T. Seidensticker, and M. Steinhauser, Phys. Lett. B **426**, 125 (1998).
[44] T. Seidensticker, in *6th International Workshop on New Computing Techniques in Physics Research: Software Engineering, Artificial Intelligence Neural Nets, Genetic Algorithms, Symbolic Algebra, Automatic Calculation* (1999), arXiv:hep-ph/9905298.
[45] Up to this order, a naive Taylor expansion of the amplitude is possible except for the fermionic corrections with a closed charm quark loop. These contributions are taken over from Refs. [30,31].
[46] A. V. Smirnov and F. S. Chuharev, Comput. Phys. Commun. **247**, 106877 (2020).
[47] R. N. Lee, arXiv:1212.2685.
[48] R. N. Lee, J. Phys. Conf. Ser. **523**, 012059 (2014).
[49] R. Mertig, M. Bohm, and A. Denner, Comput. Phys. Commun. **64**, 345 (1991).
[50] V. Shtabovenko, R. Mertig, and F. Orellana, Comput. Phys. Commun. **207**, 432 (2016).
[51] V. Shtabovenko, R. Mertig, and F. Orellana, Comput. Phys. Commun. **256**, 107478 (2020).
[52] V. Shtabovenko, in *20th International Workshop on Advanced Computing and Analysis Techniques in Physics Research: AI Decoded—Towards Sustainable, Diverse, Performant and Effective Scientific Computing* (2021), arXiv:2112.14132.
[53] E. Panzer, Feynman integrals and hyperlogarithms, Ph.D. thesis, Humboldt University, 2015.
[54] C. Duhr and F. Dulat, J. High Energy Phys. 08 (2019) 135.
[55] O. Schnetz, https://www.math.fau.de/person/oliver-schnetz.
[56] K. G. Chetyrkin, M. Misiak, and M. Munz, Nucl. Phys. **B518**, 473 (1998).
[57] M. Ciuchini, E. Franco, V. Lubicz, and F. Mescia, Nucl. Phys. **B625**, 211 (2002).
[58] F. Herren and M. Steinhauser, Comput. Phys. Commun. **224**, 333 (2018).
[59] P. A. Zyla *et al.* (Particle Data Group), Prog. Theor. Exp. Phys. **2020**, 083C01 (2020).
[60] K. G. Chetyrkin, J. H. Kuhn, A. Maier, P. Maierhofer, P. Marquard, M. Steinhauser, and C. Sturm, Phys. Rev. D **96**, 116007(A) (2017).
[61] A. Bazavov, C. Bernard, N. Brown, C. DeTar, A. X. El-Khadra *et al.*, Phys. Rev. D **98**, 074512 (2018).
[62] M. Beneke, Phys. Lett. B **434**, 115 (1998).
[63] I. I. Y. Bigi, M. A. Shifman, N. G. Uraltsev, and A. I. Vainshtein, Phys. Rev. D **50**, 2234 (1994).
[64] M. Beneke and V. M. Braun, Nucl. Phys. **B426**, 301 (1994).
[65] M. Beneke, Eur. Phys. J. Special Topics **230**, 2565 (2021).
[66] R. Aaij *et al.* (LHCb Collaboration), Nat. Phys. **18**, 1 (2022).
[67] M. Bordone, B. Capdevila, and P. Gambino, Phys. Lett. B **822**, 136679 (2021).
[68] Y. Aoki *et al.*, arXiv:2111.09849.
[69] J. A. M. Vermaseren, Comput. Phys. Commun. **83**, 45 (1994).
[70] D. Binosi and L. Theussl, Comput. Phys. Commun. **161**, 76 (2004).